Strongly interacting quark-gluon plasma, and the critical behavior of QCD at imaginary μ

Massimo D'Elia,[1] Francesco Di Renzo,[2] and Maria Paola Lombardo[3]

[1]*Dipartimento di Fisica dell'Università di Genova and INFN, I-16146, Genova, Italy*
[2]*Dipartimento di Fisica dell'Università di Parma and INFN, I-43100, Parma, Italy*
[3]*INFN-Laboratori Nazionali di Frascati, I-00044, Frascati(RM), Italy*

(Received 7 June 2007; published 19 December 2007)

We explore the highly nonperturbative hot region of the QCD phase diagram close to T_c by use of an imaginary chemical potential μ which avoids the sign problem. The simulations use four flavors of staggered fermions and are carried out on a $16^3 \times 4$ lattice. The number density and the quark number susceptibility are consistent with a critical behavior associated with the transition line in the negative μ^2 half-plane. We compare the analytic continuation of these results with various phenomenological models, none of which provides a satisfactory description of data, a failure on which we make some comments. These results complement and extend the information obtained via the analysis of the susceptibilities evaluated at zero μ, yielding a simple description of the candidate strongly interacting quark-gluon plasma phase. As a byproduct of our analysis we investigate the Polyakov loop and its hermitian conjugate. Our data offer vivid evidence of the importance of the complex nature of the functional integral measure, which results in $L(\mu) \neq \bar{L}(\mu)$ for a real chemical potential μ.

DOI: 10.1103/PhysRevD.76.114509 PACS numbers: 12.38.Gc, 11.15.Ha, 12.38.Mh

I. INTRODUCTION

Theoretical arguments and experimental evidence suggest that hadronic matter undergoes a transition to a plasma of quarks and gluons at high temperature [1]. At extremely high temperatures quarks and gluons are nearly free, and should be described by the Stefan-Boltzmann law with the appropriate degrees of freedom. When temperature is not much higher than the critical temperature—say, $T_c < T < \simeq 2T_c$—strong interactions among the constituents give rise to nonperturbative effects. In short, at large T the quark-gluon plasma (QGP) is a gas of nearly free quarks, which becomes strongly interacting at lower temperatures $T = (1 - 3)T_c$ [2,3].

Several proposals have been made to characterize the properties of the system in such a nonperturbative phase. For instance the above-mentioned strong interactions might be enough to preserve bound states above T_c, while colored states might appear, deeply affecting the thermodynamics of the system [4]. Analytic techniques are being refined more and more, so as to be able to capture the features of the system closer and closer to T_c [5]. Model theories of quasiparticle physics have been considered as well [6,7]. In this work we study this interesting dynamical region by lattice QCD simulations at $T \simeq 1.1T_c$ (the reason for this choice will be clear in the following), and a nonzero baryon density.

In principle, lattice QCD simulations at nonzero baryon density are plagued by the sign problem [8]. However, it has been realized that this problem can be circumvented thanks to physical fluctuations, which grow relatively large in the quark-gluon plasma phase. In this work we adopted the imaginary chemical potential approach [9–16], which avoids the sign problem and makes possible conventional lattice QCD simulations. The interested reader might want to consult Refs. [17,18] for recent reviews and [19,20] for more pedagogical introductions into the subject.

Other studies in the quark-gluon plasma phase have addressed the higher temperature regime [21–25]. Here we analyze in detail the nonperturbative behavior close to T_c, in the candidate strongly coupled quark-gluon plasma (sQGP) region (some preliminary results have appeared in [26]). We note that in the sQGP region the chiral critical line lies in the imaginary chemical potential plane, and that such a chiral line ends in the proximity of the endpoint of the Roberge-Weiss line [27]. We focus our analysis on the particle number and its susceptibility, on the chiral condensate, and on the Polyakov loop, and we find that the results are consistent with those expected of a critical behavior associated with the critical line at imaginary chemical potential. Hence, the numerical results are compatible with simple power law behavior of the equation of state as a function of the imaginary chemical potential μ_I, yielding a modified form of the Stefan-Boltzmann law.

The rest of this paper is organized as follows. Section II is devoted to the analysis of the particle number and the chiral condensate, which are related by the Maxwell equation. In Sec. III we discuss the behavior of the Polyakov loop. It turns out that our approach offers a particularly simple description of an apparent puzzle, and, at the same time, gives direct evidence of the phase of the determinant at nonzero, real chemical potential. The implications on the equation of state are summarized in Sec. III, while Sec. IV discusses our results in the light of phenomenological proposals, and alternative lattice approaches. The last section is a short summation.

II. THERMODYNAMICS OF THE HOT PHASE CLOSE TO T_c

Let us remind ourselves of the critical lines in the phase diagram in the T, μ^2 plane (Fig. 1): at high temperature there is the Roberge-Weiss transition at $\mu = \pi T/3$, associated with the phase of the Polyakov loop, ending at $T = T_{\rm RW}$. At lower temperatures the QGP region is limited by a chiral transition at negative μ^2, which continues into the physical chiral transition at positive μ^2, i.e., real chemical potential [11,12].

While μ approaches $\pi T/3$ at a constant temperature $T \simeq T_{\rm RW}$, one approaches the point where the chiral transition meets (within errors) the Roberge-Weiss transition. Within the current numerical accuracy the endpoint of the two transitions cannot be resolved, and the nature of the critical behavior around $T = T_{\rm RW}$, $\mu = \pi T/3$ is an interesting question in itself. If T is slightly larger than $T_{\rm RW}$ we are approaching the Roberge-Weiss transition, if slightly lower we hit the chiral transition, and at $T = T_{\rm RW}$ we might expect interesting critical phenomena whose universality class is not known *a priori*. Note that in the chiral limit the $\mu = 0$ transition should be of first order, and we do not expect any tricritical point along the critical line at a real chemical potential. A possible occurrence of an endpoint at finite mass in the T, μ plane depends on dynamical details, which are not known, and are not relevant for the present study.

We have then carried out simulations on a $16^3 \times 4$ lattice using four flavors of staggered fermions at $\beta = 5.1$, which, according to our previous results [12], yields $T \simeq T_{\rm RW}$, endpoint of the Roberge-Weiss (RW) transition,. Fermions are fully degenerate, with a bare dimensionless mass (a being the lattice spacing) $\hat{m} \equiv ma = 0.05$. Previous work indicates that this lattice with $N_t = 4$is

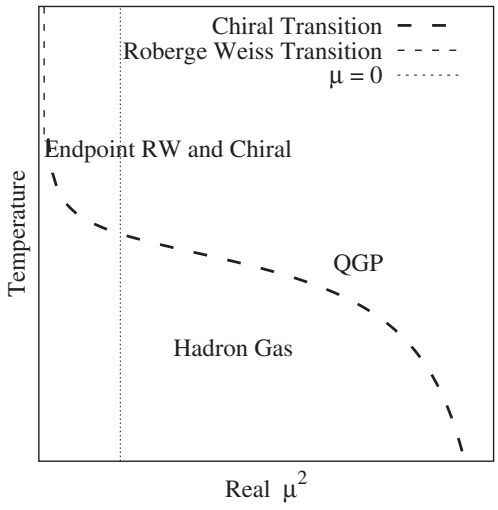

FIG. 1. Schematic phase diagram for four-flavor QCD in the T, μ^2 plane. The candidate sQGP phase is bound by the chiral (pseudo)critical line in the negative μ^2 half-plane.

coarse (opposed to fine). On a coarse lattice we need quark masses $ma \leq 0.025$ to show behavior representative of QCD in the chiral limit [28].

For $N_f = 4$ the finite temperature, zero density transition is of first order in the chiral limit. Earlier work [28] suggests that the critical value of the mass $m_c a$ above which the transition disappears satisfies $0.05 > m_c a > 0.2$, and our previous results confirm that the transition remains of first order at $ma = 0.05$. So we do not expect any endpoint in the T, μ plane for this mass value.

We used a standard hybrid Monte Carlo algorithm: note that with an imaginary chemical potential the standard trick of reducing the number of flavors via an even-odd partitioning still applies. So we can simulate four-continuum flavor using $M^\dagger M$ in the measure, without taking the square root.

We note that existing parametrization can successfully describe the data for a small chemical potential. Here, we examine all the available intervals of chemical potential, from zero to the RW transition, taking data for 26 μ_I values. For each μ we performed $O(10^4)$ unit length trajectories, measuring each of five of them.

For our lattice the value of the (dimensionless) $\hat{\mu} \equiv \mu a$ which is relevant for the Roberge-Weiss transition reads $\hat{\mu} = \pi/12$ (the temperature being $T = 1/(aN_t)$ and in our case $N_t = 4$). With a slight abuse we will omit in the following the hat-notation, nevertheless measuring μ and T in unit of inverse lattice spacing.

First, we check our data for the particle number against a simple free field behavior. We have numerically computed the free field results for real chemical potential on a $16^3 \times 4$ lattice, and $m_q = 0.05$, and we have fitted them to an expression motivated by one-dimensional QCD [29], which turns out to be an excellent parametrization:

$$n(\mu)_{\rm free} = \frac{3\sinh(\mu/T)}{K + \cosh(\mu/T)}. \tag{1}$$

where K is a fit parameter, yielding the free field results for the number density as a function of imaginary chemical potential

$$n(\mu_I)_{\rm free} = \frac{3\sin(\mu_I/T)}{K + \cos(\mu_I/T)}. \tag{2}$$

We then considered the ratio between the numerical results and such free field results, $R_F(\mu_I) = n(\mu_I)/n(\mu_I)_{\rm free}$ (Fig. 2). We observe a clear dependence of $R_F(\mu_I)$ on μ_I: the results are qualitatively different from a free field, and the discrepancy cannot be accounted for by any simple renormalization of the degrees of freedom. This behavior should be contrasted with that of Fig. 12 of Ref. [22], where the results at high temperature did differ from a free field behavior by a constant factor very close to 1.

As a second attempt at interpreting our data in terms of the simplest parametrizations, we consider an analogy with

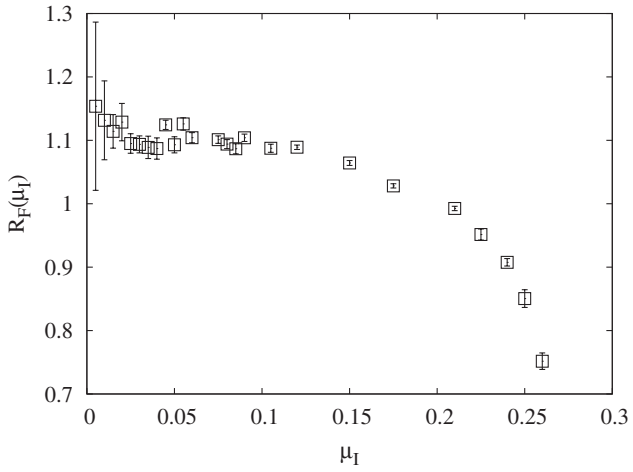

FIG. 2. $R_F(\mu_I) = n(\mu_I)/n(\mu_I)_{\text{free}}$ as a function of μ_I, showing very clear evidence of a deviation from a free field behavior.

the hadron resonance gas (HRG) model [30,31]. We will discuss more fully these aspects in the last section.

In a nutshell, the HRG model describes the system as a gas of weakly interacting resonances. The pressure of the HRG model reads:

$$\frac{P(T,\mu) - P(T,0)}{T^4} \simeq F(T)\left(\cosh\left(\frac{N_c\mu}{T}\right) - 1\right) \tag{3}$$

$$F(T) \simeq \int dm\rho(m)\left(\frac{m}{T}\right)^2 K_2\left(\frac{m}{T}\right), \tag{4}$$

and the argument of the hyperbolic cosine, $(N_c\mu/T)$, tells us that in the hadronic phase one can only excite baryonic degrees of freedom.

Let us remind ourselves here that general arguments guarantee that the partition function is periodic at imaginary μ, and that the strong coupling analysis shows that periodicity is smooth at low temperature. Hence, the number density reads [12]

$$n(\mu_I) = \sum_k b_k^F \sin(kN_cN_t\mu_I). \tag{5}$$

When HRG holds true, one term in the Fourier series should suffice:

$$n(\mu_I) = \frac{\partial P(\mu)}{\partial\mu} = K(T)\sin(N_cN_t\mu_I). \tag{6}$$

Previous comparisons with the hadron resonance gas model used the Taylor expansion of the thermodynamics observables. In order to make sure that a Taylor series does indeed converge to the appropriate trigonometric function, one would have, in principle, to compute an infinite number of terms, where, at the best, only the first six terms of the series have been computed [31]. Obviously, the Fourier analysis—which is automatic within the imaginary chemical potential approach—needs only one parameter fit to assess the validity, or lack thereof, of the HRG parametrization.

In Fig. 3 we display the ratios

$$R_B(\mu_I) = \frac{n(\mu_I)}{\sin(3\mu_I/T)} \tag{7}$$

$$R_q(\mu_I) = \frac{n(\mu_I)}{3\sin(\mu_I/T)}. \tag{8}$$

$R_B(\mu_I)$ should be a constant for a simple hadron gas (cf. again Ref. [22]), while, mutatis mutandis, $R_q(\mu_I)$ should be a constant for a "hadron gas" made of quarks. Both R_B and R_q stay constant only for a short interval of chemical potential, indicating the region where $n(\mu_I) \propto \mu_I$. The deviation from a linear behavior (for $\mu_I > 0.05$), as well as from the simplest trigonometric parametrizations (for $\mu_I > 0.15$), are evident from the plot.

We now move on and propose to describe the particle number in the critical region as

$$n(\mu_I) = A\mu_I(\mu_I^{c2} - \mu_I^2)^\alpha. \tag{9}$$

This ansatz for $n(\mu_I)$ takes into account that $n(\mu)$ should be an odd function of μ. Moreover, it reproduces a singular behavior of the quark number susceptibility at a genuine critical point. Namely, the most divergent part of the quark number susceptibility χ_q behaves as

$$\chi_q(\mu_I) \propto \frac{1}{(\mu_I^{c2} - \mu_I^2)^\gamma} \tag{10}$$

where $\gamma = 1 - \alpha$, while $\mu_I^c = \pi/12$ if the critical point coincides with the Roberge-Weiss line.

We then fit our data to Eq. (9) with μ_I^c either open or constrained. A fit to our entire interval with unconstrained

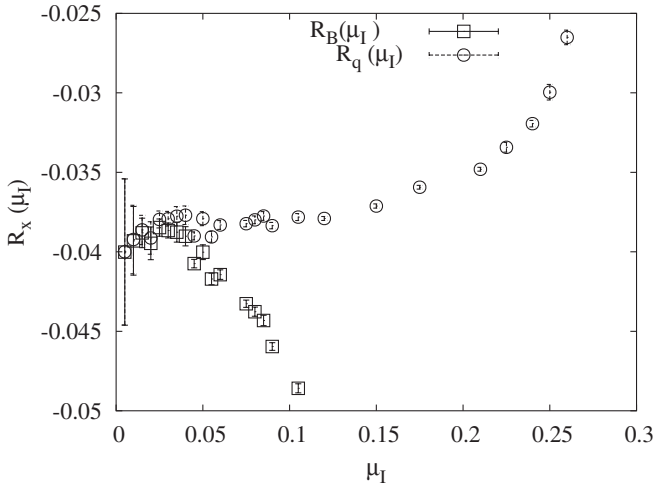

FIG. 3. $R_x(\mu_I)$ (defined in Eqs. (7) and (8)) as a function of μ_I, showing the limitations of a linear approximations, as well as the deviations from the simplest trigonometric parametrizations motivated by a hadron resonance gas model.

μ_I^c gives $A = -0.94(4)$, $\mu_I^{c2} = 0.0804(2)$, $\alpha = 0.28(2)$ with a reduced $\tilde{\chi}^2 = 2.4$. This is the fit to all data shown in Fig. 4.

We checked the stability of these results by choosing different ranges in chemical potential, and we obtained the exponent α ranging between 0.34(8) and 0.26(3), μ_I^{c2} between 0.078(4) and 0.091(12), with reduced $\tilde{\chi}^2$ ranging between 1.8 and 5.

If we constrain $\mu_I^{c2} = (\pi/12)^2$ the quality of the fits decreases giving a reduced $\tilde{\chi}^2 \simeq 12$. If we limit the fitting interval to $\mu_I > 0.15$, we need to add a constant to the function to approximate the regular component. In practice, we fit to

$$n(\mu_I) = A\mu_I(\mu_I^{c2} - \mu_I^2)^\alpha + B. \tag{11}$$

We obtain $A = -0.54(4)$, $\alpha = 0.14(1)$, $B = -0.010(3)$, a reduced $\tilde{\chi}^2 = 1.79$. This is the second fit shown in Fig. 4.

We also consider a critical behavior supplemented by a regular linear term:

$$n(\mu_I) = A\mu_I(\mu_I^{c2} - \mu_I^2)^\alpha + B\mu_I. \tag{12}$$

This form of the regular term respects the symmetries of $n(\mu)$ and hence can be used for analytic continuation, at variance with the simple modification considered above, when we supplemented $n(\mu)$ by a constant. The results for this fit are $A = -1.04(7)$, $\mu_I^2 = 0.62(7)$, $\alpha = 0.62(7)$, and $B = -0.26(4)$, with a reduced $\chi^2 = 1.74$.

For the purpose of illustrating the systematics associated to the analytic continuation, we have also performed simple polynomial fits. We postpone to the last section a discussion of the analytic continuation, and we now go back to the quark number susceptibility as entailed in Eq. (10), for which our results indicate $\gamma = 1 - \alpha \simeq 0.7$. Figure 5 shows χ_q obtained by numerical differentiation of $n(\mu_I)$. Note that $n(\mu_I)$ is a decreasing function of μ_I, hence the quark number susceptibility is a negative function. The numerical quality is of course poor, but, anyway, a fit to the form of Eq. (10) with an open μ_I^c gives $\gamma = 0.66(16)$, while a fit with constrained μ_I^c gives $\gamma = 0.44(22)$, in agreement with the above estimates, within the large errors.

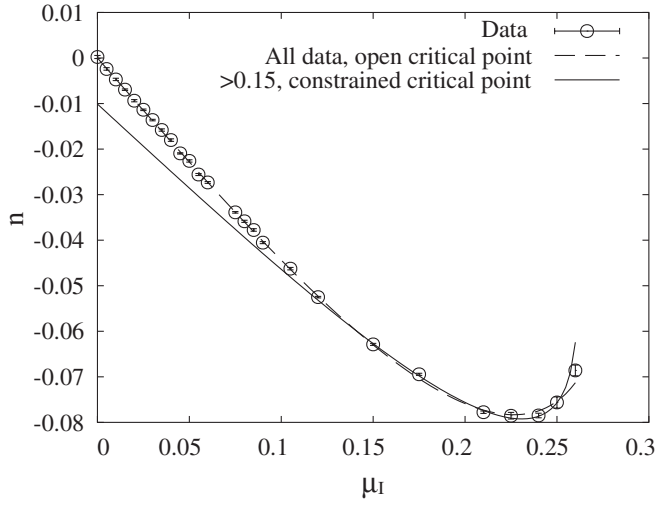

FIG. 4. $n(\mu)$ fitted to the form predicted by the simple critical behavior at imaginary μ (Eq. (9)).

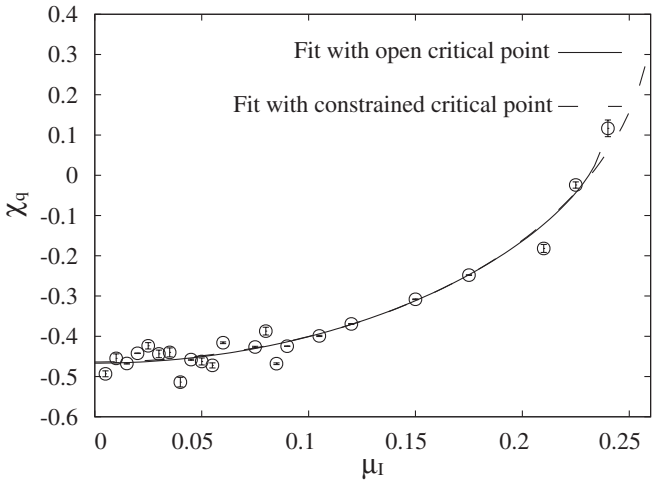

FIG. 5. The quark number susceptibility obtained by numerical differentiation of the results for the quark number.

The chiral condensate $\langle\bar{\psi}\psi\rangle$ can be inferred from the chiral equation of state in either phase, and also in the presence of an explicit chiral symmetry breaking term. To make a closer contact with thermodynamics, we consider the Maxwell relations (the temperature is constant and its dependence is omitted) [32]:

$$\frac{\partial n(\mu, m)}{\partial m} = \frac{\partial\langle\bar{\psi}\psi\rangle(\mu, m)}{\partial\mu}. \tag{13}$$

Considering the m dependence in the expression for $n(\mu, T)$,

$$n(\mu, m) = F(m)\mu(\mu_I^{c2}(m) - \mu^2)^\alpha \tag{14}$$

where $F(m)$ depends only on the quark mass, and using Eq. (13) we arrive at

$$\langle\bar{\psi}\psi\rangle(\mu) = H(m)(\mu_I^{c2}(m) - \mu^2)^{\alpha+1} + K(m)(\mu_I^{c2}(m) - \mu^2)^\alpha + \langle\bar{\psi}\psi\rangle_0 \tag{15}$$

where $H(m)$, $K(m)$ depends only on the mass and $\langle\bar{\psi}\psi\rangle_0$ is an integration constant which can be fixed, e.g., by the chiral condensate at zero chemical potential.

We have then fitted the chiral condensate to the leading term at $\mu \simeq \mu_c$,

$$\langle\bar{\psi}\psi\rangle = K(b - \mu^2)^{\alpha_c} + A, \tag{16}$$

obtaining a nice fit with a reduced $\tilde{\chi}^2 = 0.79$, $A = 0.552(6)$, $b = 0.06628(8)$, $K = -0.63(2)$, and $\alpha_c = 0.47(2)$ in reasonable agreement with α estimated from the number density. By constraining the fitting interval $\mu_I > 0.2$ the subleading contributions are less important,

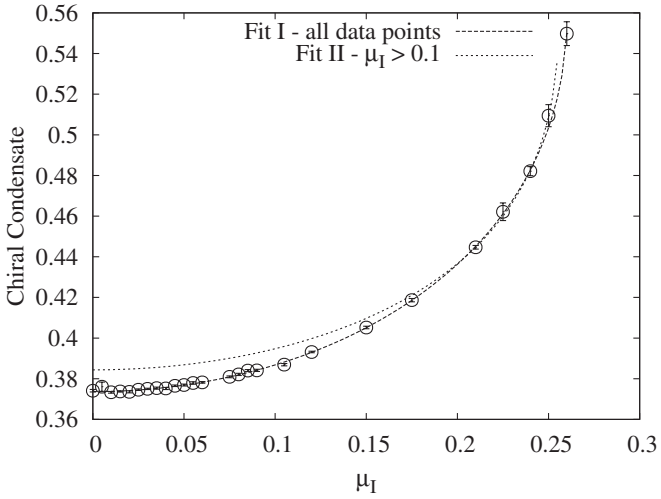

FIG. 6. Numerical results for the chiral condensate, and the results of the fit to a functional form inferred from the Maxwell equation (Eq. (13)).

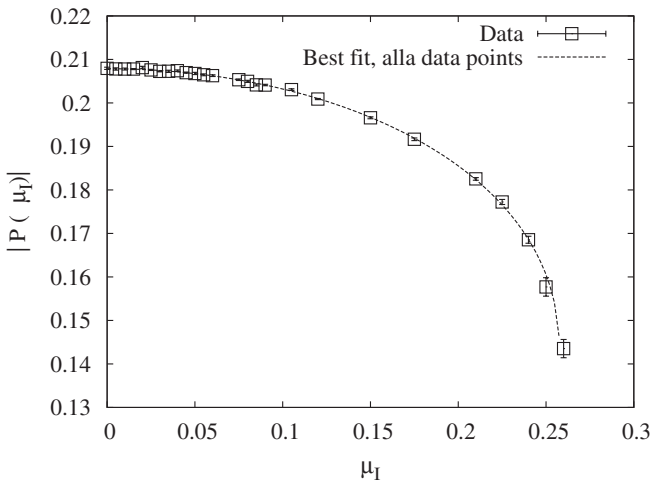

FIG. 7. The Polyakov loop fitted to the form predicted by a simple critical behavior at imaginary μ (Eq. (17)).

and $\alpha_c = 0.32(12)$ gets even closer to α. The numerical results for the chiral condensate and the fits described above are shown in Fig. 6.

It might be interesting to compare this critical behavior with that of the endpoint of QCD from model field theories [33–35].

III. THE POLYAKOV LOOP

In the same spirit we have fitted the traced Polyakov loop $L = \langle \mathrm{Tr} P \rangle$ to a power law form:

$$L(\mu_I) \propto (\mu_I^{c2} - \mu_I^2)^{\beta}. \tag{17}$$

Figure 7 displays the results of the fit of the absolute value of the Polyakov loop, which indeed looks satisfactory.

It is interesting to look in more detail into the behavior of $L = \langle \mathrm{Tr} P \rangle$.

The Polyakov loop P satisfies the same relation as the quark propagator at nonzero chemical potential [36]:

$$P(\mu) = P^{\dagger}(-\mu). \tag{18}$$

This relation implies that, while both $L = \langle \mathrm{Tr} P \rangle$ and $\bar{L} = \langle \mathrm{Tr} P^{\dagger} \rangle$ are real at real chemical potential, $L \neq \bar{L}$, as noted in [25,37–40]. We will show that the results at imaginary chemical potential offer a particularly simple illustration of these ideas, as well as direct evidence of the complex phase of the determinant.

The asymmetry at real chemical potential is easily understood by considering the distribution of the Polyakov loops in the complex plane for $\mu = 0$, since the Z_3 center symmetry is broken by the dynamical quarks, the root corresponding to the phase $\phi = 0$ is preferred, and the average is nonzero. A nonzero, positive chemical potential encourages forward propagation: the distribution of the phases is further peaked at $\phi = 0$, while the two other phases have the same probability. Hence, the Polyakov loop remains real, and the final average is again real, different from zero, and slightly larger than the one at zero density. $\bar{L}$ instead describes backward propagation: again the Polyakov loop remains real, however its length is reduced, hence $L(\mu) \neq \bar{L}(\mu)$.

Notice that at a first naive look it may sound strange that while configuration by configuration the Polyakov loop and its hermitian conjugate are always the complex conjugate of each other, their expectation values, even being real, differ from each other. However it should be clear that the complex nature of the functional integral measure plays an essential role in this respect, since the real part of the expectation value is not just the expectation value of the real part. In that sense the fact that $L(\mu) \neq \bar{L}(\mu)$ is directly linked to the complex nature of the fermion determinant, thus also giving a qualitative feeling about the severeness of the sign problem (for analogous interpretations of the complex phase continued to $\mu^2 < 0$, see also Refs. [8,41,42]).

An apparent puzzle then arises when one considers the behavior at imaginary chemical potential: there the measure is real and one can show that the absolute value of L and $\bar{L}$ are equal as well as their real parts. What is then the fate of the asymmetry, which is present at real chemical potential?

Consider

$$L_{o/e}(\mu) \equiv L(\mu) \pm L(-\mu) = L(\mu) \pm \bar{L}(\mu), \tag{19}$$

where Eq. (18) has been used in the last equality. $L_{o/e}$ are, respectively, even and odd in μ. Remember that the analytic continuation to imaginary chemical potential of an even function is real, while the analytic continuation of an odd function is purely imaginary. Hence, the analytic continuation of the even observable $L_e(\mu) = L(\mu) + \bar{L}(\mu)$ at imaginary chemical potential is the real part of

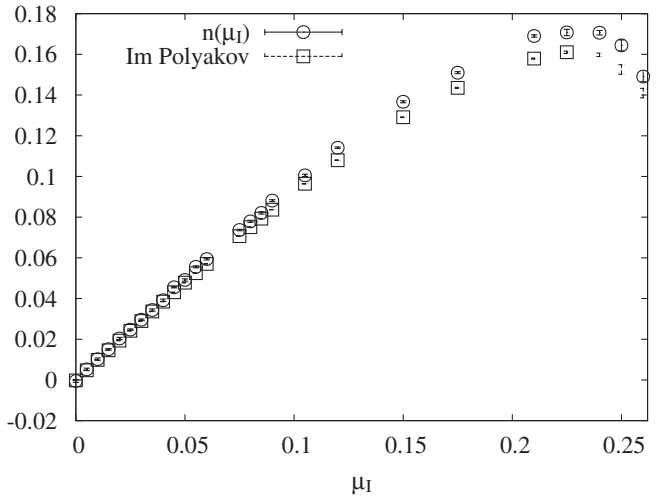

FIG. 8. The imaginary part of the Polyakov loop, divided by the coefficient of the linear term of a fit at small μ, as a function of the imaginary chemical potential, demonstrating the relevance of the phase of the determinant for a real chemical potential; in the same plot we show the number density, again normalized by the coefficient of the linear term.

$L(\mu_I)$; while the analytic continuation of $L_o(\mu) = L(\mu) - \bar{L}(\mu)$ is the imaginary part of $L(\mu_I)$ at imaginary μ. L itself has no definite μ-parity and its analytic continuation develops an imaginary part.

We conclude that we must search for the analytic continuation of the asymmetry $L \neq \bar{L}$, which is present at real chemical potential in the imaginary part of the Polyakov loop, which is nonzero in presence of an imaginary chemical potential. Figure 8 shows the imaginary part of $L(\mu_I)$: it is different from zero, offering clean, direct evidence of the asymmetry $L \neq \bar{L}$, hence of the complex phase of the determinant at real chemical potential. In the same Fig. 8 we have also plotted $n(\mu_I)$ (both L and n with an appropriate normalization), to show its correlation with $L(\mu_I)$. This correlation is in agreement with the lattice interpretation of the number operator n as "counting" the links winding forwards minus those winding backwards, and it should become exact in the heavy quark limit when the model reduces to a Polyakov loop model [43,44].

Let us now come back to the critical behavior of $|L|$: since $\mathrm{Im}(L(\mu_I) \propto n(\mu_I))$, we might expect that $|L(\mu_I)|$ approaches zero with a similar power law. The fit of Fig. 7 gives an exponent of 0.45(2), in the same range as γ. It would be interesting, of course, the study of the string tension and other correlators in the same range of chemical potentials.

IV. ANALYTIC CONTINUATION

Let us remind ourselves that general arguments guarantee that the analytical continuation $f(x)$ is unique in the analyticity domain. In practice, however, $f(x)$ is unknown and has to be approximated by some series expansion or suitable ansatz. In either case, one has to pay attention to the fact that, by modifying the original expression by a nonleading term, the difference in physical quantities is still nonleading. We refer to our earlier publications [12,19,22] for a more complete discussion of these points, including the usage of Padé approximants to improve the convergence [16,45].

When these considerations are applied to the case at hand, we conclude that we do not expect that the singular critical behavior of a quantity is able to describe the quantity far from the critical regime (where the regular terms become dominant).

The region where the leading critical behavior describes correctly the data is not known *a priori*. It might well be that subleading regular contributions play some role. To address this point we compare the analytic continuation obtained by use of different parametrizations.

In Fig. 9 we show the analytic continuated curves obtained from the fits described in Sec. II above, as an indicator of systematic errors. For each curve we also draw associated error bands, coming from statistical errors alone.

As expected, all the results agree well with each other until $\mu = |\mu_c|$, the critical point at imaginary chemical potential which defines the radius of convergence. In this region the systematic errors are below the statistical ones.

For $\mu > \mu_c$ the Taylor series does not seem to converge, confirming that the distance from the nearest singularity defines the radius of convergence of the Taylor series. This contrasts with the behavior of the two fits which contain a term associated with a critical behavior.

From Fig. 9 we infer that the analytic continuation of the fit functions which took into account a singularity seem reasonably stable under variations of the regular contribu-

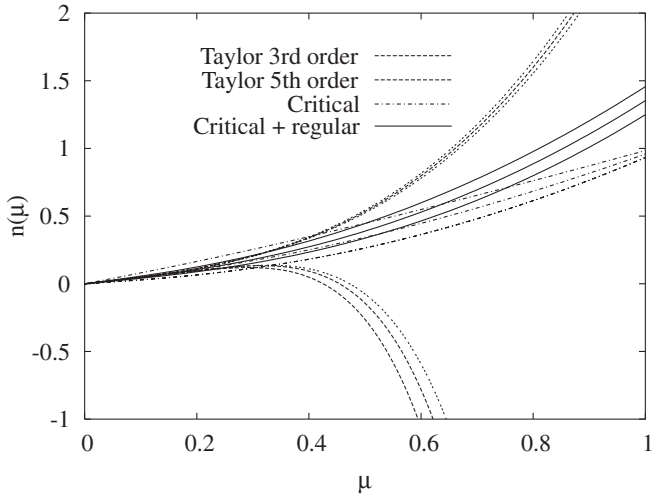

FIG. 9. Analytic continuation to real chemical potential of $n(\mu)$ based on the fits at imaginary μ described in Sec. II, together with the associated error bands.

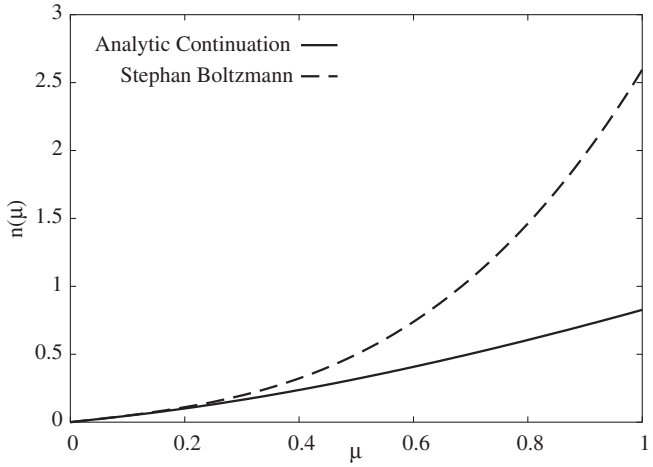

FIG. 10. $n(\mu)$ from analytic continuation, together with a free field behavior is shown for comparison. The fits suggest that the slower increase observed in the interacting case with respect to the free case can be described by an overall exponent smaller than 1.

tion, i.e., the regular term remains subleading at least until $\mu < 1.$, i.e., $\mu/T < 4$.

Let us then compare

$$n(\mu) = A\mu(\mu_I^{c2} + \mu^2)^{\alpha} \tag{20}$$

with $\alpha \simeq .4$ with a simple Stefan-Boltzmann behavior.

The results are shown in Fig. 10. Note that coefficient A has a nontrivial dimension, again indicating that the system is not free.

It is then amusing to notice that by using simple arguments from the theory of critical phenomena we arrive at a modified (lattice) Stefan-Boltzmann law, which would correspond to $\alpha = 1$, and a large $\mu_I^{c2} \simeq 0.5$. In this framework a large μ_I^c can be interpreted as a spinodal point at imaginary chemical potential far away from the Roberge-Weiss line.

Obviously, Eq. (20) accounts for a slower increase of the particle density closer to T_c than in the free case. This is expected on physical grounds, as well as from the behavior of the susceptibilities [38,46–50], and of course accounts for the behavior observed in Fig. 2.

From the results above, we conclude that the data in the candidate region for a strongly coupled QCD are accounted for by a conventional critical behavior: clearly, a free field behavior would have been incompatible with it. In other words, the nonperturbative features of the plasma are closely related with the occurrence of the critical line at negative μ^2.

V. THERMODYNAMICS AND PARTICLE CONTENT

Early in this article we have contrasted our data with some very simple parametrizations motivated by the HRG approach. Here we discuss this point in some more detail, in particular, we wish to examine the proposal that in the deconfined, strongly interacting region considered here one might observe either colored and colorless [51] bound states: in short, at large T the QGP is a gas of nearly free quarks, which becomes strongly interacting at lower temperatures $T = (1 - 3)T_c$, see, e.g., [52,53] for recent reviews and a complete set of references.

In Ref. [24] the following parametrization was proposed for the contribution of the colored states to the subtracted pressure $\Delta P_C = P_C(T, \mu) - P_C(T, 0)$ (we slightly simplify the notation):

$$\begin{aligned}\frac{\Delta P_C}{T^4} = {} & (F_q(T))((\cosh(\mu_u/T) - 1) + (\cosh(\mu_d/T) - 1)) \\ & + F_{qq}(T)((\cosh(2\mu_u/T) - 1) + (\cosh(2\mu_d/T) - 1) \\ & + (\cosh((\mu_u + \mu_d)/T) - 1).\end{aligned} \tag{21}$$

The susceptibilities at zero chemical potential can be easily computed from Eq. (21), and we recognize that their ratios allow the identifications of the relevant degrees of freedom. This prediction for the susceptibilities ratio was contrasted with the numerical results, finding a poor agreement.

The imaginary chemical potential approach gives the possibility to check directly the consistence of various phenomenological models by analytically continuing from real to imaginary μ. We can subject our data to the same analysis by analytically continuing Eq. (21) from real to imaginary chemical potential. Setting $\mu_{\rm isospin} = \mu_u - \mu_d = 0$, and including the contribution from baryons and tetraquarks we get:

$$\begin{aligned}\frac{\Delta P}{T^4} = {} & F_q(T)(\cos(\mu/T) - 1) + F_{qq}(T)(\cos(2\mu/T) - 1) \\ & + F_{qqq}(T)(\cos(3\mu/T) - 1) \\ & + F_{qqqq}(T)(\cos(4\mu/T) - 1)\end{aligned} \tag{22}$$

giving in turn:

$$\begin{aligned}n(\mu_I, T) = {} & F_q(T)\sin(\mu_I/T) + 2F_{qq}(T)\sin(2\mu_I/T) \\ & + 3F_{qqq}(T)\sin(3\mu_I/T) \\ & + 4F_{qqq}(T)\sin(3\mu_I/T).\end{aligned} \tag{23}$$

From the point of view of the imaginary chemical potential analysis, checking these forms corresponds to performing a Fourier analysis of our results. We have then fitted our data to the form

$$n_K(\mu_I) = \sum_{j=1}^{K} F_j \sin(j\mu_I/T). \tag{24}$$

The results of the fits are shown in Fig. 11. The reduced $\tilde{\chi}^2$ ranges from 84 to 2.85 (F_1 to F_4), but the errors on the parameters grow big and the parameters themselves are not stable. Wesummarizee the results in Table I, and we conclude that, even if the trigonometric fits might eventually

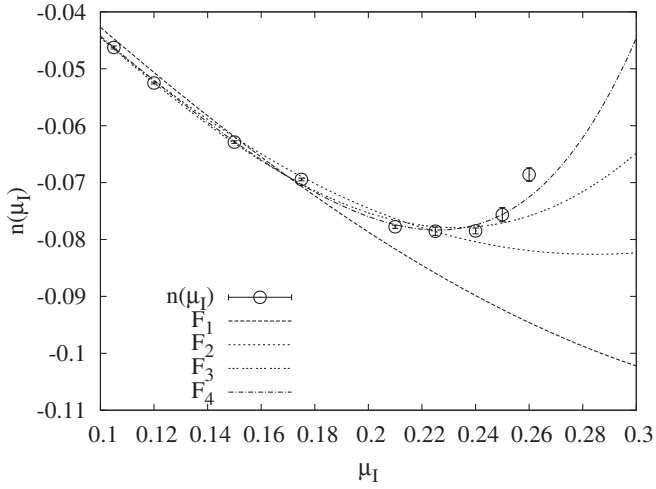

FIG. 11. Results of the fits of $n(\mu_I)$ to the trigonometric functions (Eq. (24)), see text for details.

converge, it is hard to attach any simple physical interpretation of the parameters F_1, F_2, F_3, F_4 as contribution from free quarks, diquarks, baryons, and tetraquarks.

This result is not unexpected, as the Fourier parametrization (Eq. (24)) is not compatible with the critical fits (Eq. (9)). Does this mean that the occurrence of colored bound states is ruled out?

Not really: apart from the fact that extending a hadron resonance gas description to colored states is a nontrivial assumption anyway, given the nontrivial interactions that one could expect, we should also consider that the masses themselves might well depend on the chemical potential [6,54]—the so-called Bluhm-Kampfer-Soff (BKS) effect. From the perspective of the present study, the BKS effect is indeed very natural, in view of the phase diagram in Fig. 1, and the related analysis of the data in terms of critical behavior which we have presented above. Remember, in fact, that the coefficients of the hadron gas parametrization in Eq. (21) above represent the contribution of the spectrum of resonances, hence their temperature dependence is inferred from one of the masses.

For instance, in Ref. [4] it was proposed that

$$M_{\text{coloured}} \approx 11.5T_c((T/3T_c)^{0.5} + 0.1T_c/(T - T_c)) \quad (25)$$

yielding the decoupling of the colored masses at the critical point. A similar decoupling should take place at the critical line at negative μ^2, which is not compatible with the simple factorization of the terms depending on temperature and fugacities implied by the HRG model (Eq. (21)).

In Ref. [54] it was underscored that if the derivatives of the masses with respect to the chemical potential

$$M''(T) = \frac{\partial^2 M(T,\mu)}{\partial \mu^2} \qquad (T, \mu = 0) \qquad (26)$$

are large enough, the simple interpretation of the zero chemical potential susceptibilities as probes of particle contents has to be revised, and, more generally, the decoupling of the prefactor and the simple trigonometric factors predicted by the HRG model is no longer true. Hence, we cannot use simple forms as those of Eq. (21) to assess the particle content of the sQGP gas.

Our analysis supports this point of view. It is interesting to note that a recent direct calculation [55] of the colored spectrum indicates the survival of heavy colored states above T_c. Of course the binding mechanisms and the dissociation patterns for heavy quarks and light quarks are different.

TABLE I. Parameters of the Trigonometric Fits.

F_1	F_2	F_3	F_4	χ^2/d.o.f.
−0.110(1)	···	···	···	84
−0.071(3)	−0.023(2)	···	···	11.11
0.028(15)	−0.114(14)	0.029(4)	···	4.18
0.43(11)	−0.55(13)	0.257(66)	−0.049(14)	2.85

VI. SUMMARY AND OUTLOOK

We have studied the critical behavior of the system in proximity of the critical endpoint of the chiral and RW line in the negative μ^2. We have given a simple description of the nonperturbative features of the sQGP phase, based on the analysis of the critical behavior in the imaginary μ plane. We have proposed an equation of state of the form

$$n(\mu) = A\mu(\mu_{Ic}^2 + \mu^2)^\alpha$$

with $\alpha \simeq 0.3$, which accounts nicely for all the features of the numerical data. The exponent would read $\alpha = 1$ for a Stefan-Boltzmann-like law.

The results thus obtained should be valid in the entire analiticity domain. Practical limitations—discussed at length in previous work—do arise because of numerical accuracy.

As for the particle content of the system, our results suggest that a fit to

$$\frac{\Delta P}{T^4} = F_q(T)(\cos(\mu/T) - 1) + F_{qq}(T)(\cos(2\mu/T) - 1) + F_{qqq}(T)(\cos(3\mu/T) - 1) + F_{qqqq}(T)(\cos(4\mu/T) - 1)$$

cannot afford any definite conclusion. This does not come as a surprise. The masses themselves, hence the coefficients, will depend on μ in some complicated way, which should anyhow conjure to give the simple behavior observed in the data. The fact that the masses themselves should depend on the chemical potential while approaching the critical endpoint offers a simple realization of the BKS mechanism. It should also be pointed out that extending a hadron resonance gas description to colored states is a

nontrivial assumption anyway, given the nontrivial interactions that one could expect.

It would be very interesting to confront the numerical results in a broader range of temperatures with these ideas, as well as with analytic calculations and phenomenological models. Future work should hopefully be able to give a coherent account of critical behavior, high temperature expansions, and particle contents in the region of the strongly interacting quark-gluon plasma. We hope that the simple description offered here might be of help in building such a complete picture.

ACKNOWLEDGMENTS

We wish to thank Claudia Ratti, Burkhardt Kämpfer, Aleksi Vuorinen, Francesco Becattini, and Philippe de Forcrand for helpful conversations and correspondence. We acknowledge partial support from the Galileo Galilei Institute in Florence, under the *High Density QCD* program. The numerical simulations were carried out on the APEmille computer installed in Milano-Bicocca, and we would like to thank our colleagues in Milano and Parma for their kind support.

[1] M. A. Stephanov, Proc. Sci., LAT2006 (2006) 024 [arXiv:hep-lat/0701002].
[2] E. Shuryak, arXiv:hep-ph/0703208.
[3] J. P. Blaizot, J. Phys. G **34**, S243 (2007).
[4] E. V. Shuryak and I. Zahed, Phys. Rev. D **70**, 054507 (2004).
[5] A. Ipp, K. Kajantie, A. Rebhan, and A. Vuorinen, Phys. Rev. D **74**, 045016 (2006), and references therein.
[6] M. Bluhm, B. Kampfer, and G. Soff, Phys. Lett. B **620**, 131 (2005).
[7] M. Bluhm and B. Kampfer, Proc. Sci., CPOD2006 (2006) 004 [arXiv:hep-ph/0611083].
[8] See, e.g., K. Splittorff and J. J. M. Verbaarschot, arXiv:hep-lat/0702011.
[9] M.-P. Lombardo, Nucl. Phys. Proc. Suppl. **83**, 375 (2000).
[10] A. Hart, M. Laine, and O. Philipsen, Nucl. Phys. **B586**, 443 (2000); Phys. Lett. B **505**, 141 (2001).
[11] Ph. de Forcrand and O. Philipsen, Nucl. Phys. **B642**, 290 (2002).
[12] M. D'Elia and M. P. Lombardo, Phys. Rev. D **67**, 014505 (2003).
[13] V. Azcoiti, G. Di Carlo, A. Galante, and V. Laliena, Nucl. Phys. **B723**, 77 (2005).
[14] H. S. Chen and X. Q. Luo, Phys. Rev. D **72**, 034504 (2005).
[15] L. K. Wu, X. Q. Luo, and H. S. Chen, Phys. Rev. D **76**, 034505 (2007).
[16] P. Cea, L. Cosmai, M. D'Elia, and A. Papa, J. High Energy Phys. 02 (2007) 066.
[17] C. Schmidt, Proc. Sci., LAT2006 (2006) 021 [arXiv:hep-lat/0610116].
[18] O. Philipsen, Proc. Sci., LAT2005 (2006) 016; Proc. Sci., JHW2005 (2006) 012 [arXiv:hep-lat/0510077].
[19] M. P. Lombardo, Prog. Theor. Phys. Suppl. **153**, 26 (2004).
[20] S. Muroya, A. Nakamura, C. Nonaka, and T. Takaishi, Prog. Theor. Phys. **110**, 615 (2003).
[21] Z. Fodor, S. D. Katz, and K. K. Szabo, Phys. Lett. B **568**, 73 (2003).
[22] M. D'Elia and M. P. Lombardo, Phys. Rev. D **70**, 074509 (2004).
[23] M. D'Elia, F. Di Renzo, and M. P. Lombardo, AIP Conf. Proc. **806**, 245 (2006).
[24] S. Ejiri, F. Karsch, and K. Redlich, Phys. Lett. B **633**, 275 (2006).
[25] S. Kratochvila and P. de Forcrand, Phys. Rev. D **73**, 114512 (2006).
[26] M. P. Lombardo, Proc. Sci., CPOD2006 (2006) 003
[27] A. Roberge and N. Weiss, Nucl. Phys. **B275**, 734 (1986).
[28] F. R. Brown *et al.*, Phys. Lett. B **251**, 181 (1990) and references therein.
[29] N. Bilic and K. Demeterfi, Phys. Lett. B **212**, 83 (1988).
[30] D. Toublan and J. B. Kogut, Phys. Lett. B **605**, 129 (2005).
[31] F. Karsch, K. Redlich, and A. Tawfik, Phys. Lett. B **571**, 67 (2003), and references therein.
[32] J. B. Kogut, H. Matsuoka, M. Stone, H. W. Wyld, S. H. Shenker, J. Shigemitsu, and D. K. Sinclair, Nucl. Phys. **B225**, 93 (1983).
[33] Y. Hatta and T. Ikeda, Phys. Rev. D **67**, 014028 (2003).
[34] B. J. Schaefer and J. Wambach, Phys. Rev. D **75**, 085015 (2007).
[35] B. J. Schaefer, J. M. Pawlowski, and J. Wambach, Phys. Rev. D **76**, 074023 (2007).
[36] J. B. Kogut, M. P. Lombardo, and D. K. Sinclair, Phys. Rev. D **51**, 1282 (1995).
[37] F. Karsch and H. W. Wyld, Phys. Rev. Lett. **55**, 2242 (1985).
[38] C. R. Allton *et al.*, Phys. Rev. D **66**, 074507 (2002); **68**, 014507 (2003).
[39] A. Dumitru, R. D. Pisarski, and D. Zschiesche, Phys. Rev. D **72**, 065008 (2005).
[40] S. Roessner, C. Ratti, and W. Weise, Phys. Rev. D **75**, 034007 (2007).
[41] K. Splittorff and B. Svetitsky, Phys. Rev. D **75**, 114504 (2007).
[42] S. Conradi and M. D'Elia, Phys. Rev. D **76**, 074501 (2007).
[43] T. C. Blum, J. E. Hetrick, and D. Toussaint, Phys. Rev. Lett. **76**, 1019 (1996).
[44] R. De Pietri, A. Feo, E. Seiler, and I. O. Stamatescu, Phys. Rev. D **76**, 114501 (2007).
[45] M. P. Lombardo, Proc. Sci., LAT2005 (2006) 168 [arXiv:hep-lat/0509181].
[46] S. Gottlieb, W. Liu, D. Toussaint, R. L. Renken, and R. L. Sugar, Phys. Rev. D **38**, 2888 (1988).
[47] C. Bernard *et al.* (MILC Collaboration), Nucl. Phys. B, Proc. Suppl. **119**, 523 (2003).

[48] R. V. Gavai and S. Gupta, Phys. Rev. D **68**, 034506 (2003); arXiv:hep-lat/0303013.
[49] S. Choe *et al.*, Phys. Rev. D **65**, 054501 (2002).
[50] R. Gavai, S. Gupta, and R. Ray, Prog. Theor. Phys. Suppl. **153**, 270 (2004).
[51] P. de Forcrand *et al.* (QCD-TARO Collaboration), Phys. Rev. D **63**, 054501 (2001).
[52] E. V. Shuryak, arXiv:hep-ph/0608177.
[53] J. P. Blaizot, Nucl. Phys. **A785**, 1 (2007).
[54] J. Liao and E. V. Shuryak, Phys. Rev. D **73**, 014509 (2006).
[55] M. Doring, K. Hubner, O. Kaczmarek, and F. Karsch, Phys. Rev. D **75**, 054504 (2007).